Article

Not peer-reviewed version

Supramolecular Assemblies in Mn(II) and Zn(II) Metal-Organic Compounds Involving Phenanthroline and Benzoate: Experimental and Theoretical Studies

Mridul Boro , Subham Banik , Rosa M. Gomila , Antonio Frontera * , Miquel Barceló-Oliver , Manjit K. Bhattacharyya *

Posted Date: 16 April 2024

doi: 10.20944/preprints202404.1039.v1

Keywords: metal-organic compounds; supramolecular dimer; self-association; DFT; QTAIM; MEP

 doi:10.20944/preprints202404.1039.v1

Article

Supramolecular Assemblies in Mn(II) and Zn(II) Metal-Organic Compounds Involving Phenanthroline and Benzoate: Experimental and Theoretical Studies

Mridul Boro [1], Subham Banik [1], Rosa M. Gomila [2], Antonio Frontera [2,*], Miquel Barcelo-Oliver [2] and Manjit K. Bhattacharyya [1,*]

[1] Department of Chemistry, Cotton University, Guwahati-781001, Assam, India
[2] Departament de Química, Universitat de les Illes Balears, Crta de Valldemossa km 7.7, 07122 Palma de Mallorca (Baleares), Spain
* Correspondence: toni.frontera@uib.es (A.F.); manjit.bhattacharyya@cottonuniversity.ac.in (M.K.B.)

Abstract: Two new Mn(II) and Zn(II) metal-organic compounds of 1,10-phenanthroline and methyl benzoates *viz*. $[Mn(phen)_2Cl_2]$2-ClBzH (**1**) and $[Zn(4\text{-}MeBz)_2(2\text{-}AmPy)_2]$ (**2**) (where, 4-MeBz = 4-methylbenzoate, 2-AmPy = 2-aminopyridine, phen = 1,10-phenanthroline, 2-ClBzH = 2-chlorobenzoic acid) have been synthesized and characterized using elemental analysis, TGA, spectroscopic (FTIR, electronic) and single crystal X-ray diffraction techniques. Crystal structure analysis of the compounds reveals the presence of various non-covalent interactions which provides stability to the crystal structures. Crystal structure analysis of the compound **1** reveals the formation of supramolecular dimer of *2-ClBzH* enclathrated within the hexameric host cavity formed by the neighboring monomeric units. Compound **2** is a mononuclear compound of Zn(II) where flexible binding topologies of *4-CH_3Bz* is observed with the metal centre. Moreover various non-covalent interactions such as lp(O)-π, lp(Cl)-π, C–H···Cl, π-stacking interactions as well as N–H···O, C–H···O and C–H···π hydrogen bonding interactions are found to be involved in plateauing the molecular self-association of the compounds. The remarkable enclathration of the H-bonded 2-ClBzH dimer into a supramolecular cavity formed by two $[Mn(phen)_2Cl_2]$ complexes has been further studied theoretically using density functional theory (DFT) calculations, non-covalent interaction (NCI) plot index and quantum theory of atoms in molecules (QTAIM) computational tools. Synergistic effects have been also analysed using molecular electrostatic potential (MEP) surface analysis.

Keywords: metal-organic compounds; supramolecular dimer; self-association; DFT; QTAIM; MEP

1. Introduction

Molecular self-assembly, especially based on inorganic metal ions and organic ligands stand as a highly efficient and widely employed strategy for constructing molecular architectures. This methodology holds significant relevance in numerous fields including catalysis, sensors, semiconductor devices, luminescent materials and in biology [1–5]. Its broad application stems from the fascinating structural topologies it engenders [6–9]. A key point for the synthesis of desired network architectures requires mutual adaptation between geometries of metal ions and the selection of proper ligands as building blocks [10]. Also the structural topologies of coordination frameworks are profoundly influenced by factors such as the coordination geometry or size of metal ions, guest molecules, counterions, as well as a variety of experimental conditions like solvent choice, metal-to-ligand ratio, reaction duration, and pH levels, etc [11–15].

The scientific communities have been delving into the intricate world of supramolecular chemistry. This recent exploration has focused on unraveling various non-covalent interactions,

 doi:10.20944/preprints202404.1039.v1

including hydrogen bonding (HB), stacking, and charge transfer interactions, with particular emphasis on their implications in crystal engineering [16,17]. Also the compounds rely on the precise coordination of molecular self-assembly, which is controlled by weak non-covalent interactions viz. anion-π, cation-π, π-stacking, C–H/π, σ/π-hole, lone-pair/π, halogen bonding etc., which through their collective strength, directional control, and synergistic effects, are integral for maintaining compound stability [18–20]. The intriguing phenomenon of cooperative reciprocity among π-stacking interactions has captured the attention of researchers, especially within the framework of crystal engineering [21,22].

The art of designing coordination complexes utilizing N-donor heterocyclic organic compounds in collaboration with aromatic carboxylates still holds the attention of researchers [23,24]. 4-Mebz has attracted great interest owing to its two interesting structural features. Firstly, its multiple bridging moieties allow for diverse bonding modes with transition metal centers, leading to a plethora of structural arrangements [25]. In the second place, it can act not only as hydrogen bond donors but also as acceptors due to the existence of protonated and/or deprotonated carboxyl groups [26]. 1,10-phenanthroline (*phen*), a heterocyclic bidentate N-donor, competently generates stable coordination compounds with various transition metals on account of its chelating nature [27]. It thereby holds an exclusive place as a primary material in coordination chemistry [28–33]. The presence of electron-deficient aromatic systems in phen makes it an excellent electron acceptor capable of stabilizing metal complexes via various unconventional non-covalent interactions [34]. Pyridine-based donors differing in substituents and stereochemistry have also given rise to immense research interest in coordination chemistry due to their potential applications in diverse fields [35,36]. 2-Aminopyridine is used for the synthesis of pharmacologically active heterocyclic molecules [37]. In addition to it, with few side wings, 2-Aminopyridine alone can exhibit various pharmacological activities [38–45]. Coordination compounds of zinc involving benzoate and substituted benzoate derivatives have been reported to possess interesting structural topologies [46,47]. Manganese complexes are found to show moderate to strong inhibition against different human cancer cells in vitro [48].

The inclusion of self-assembled guests into host cavities within supramolecular architectures typically relies on both molecular association and the size of the molecules involved [49]. Non-covalent bonding in supramolecular inclusion complexes apart from demonstrating precise three-dimensional architectures, also confer intrinsic reversibility and adaptivity, enabling dynamic responsiveness to external stimuli [50–52]. The host-guest molecules' high selectivity fosters dynamic interactions within molecular self-assemblies, paving the way for the development of supramolecular soft biomaterials with intricate structures and programmable functions [53–55].

Herein, we describe the synthesis and crystal structures of two newly synthesized Mn(II) and Zn(II) metal-organic compounds incorporating phen and 4-CH_3Bz. Characterization was performed using FT-IR and electronic spectroscopy, as well as elemental and thermo-gravimetric (TG) analysis, aiming to elucidate the role of non-covalent interactions in molecular self-assembly of mononuclear coordination compounds. Through the utilization of single-crystal X-ray diffraction, we have revealed the crystal structures of the compounds. Additionally, we have investigated a range of non-covalent interactions contributing to the molecular association of these compounds. Crystal structure analysis of compound **1** demonstrates the dimerization of 2-ClBzH moieties within the lattice, followed by their enclathration within the hexameric supramolecular host cavity formed by the orderly assembly of monomeric units. Similarly crystal structure analysis of compound **2** reveals the dual coordination mode of 4-CH_3Bz with the identical metal center, elucidating their involvement in the self-aggregation of individual units, leading to the formation of unique supramolecular architectures. Moreover non-covalent interactions involving lp(O)-π, lp(Cl)-π, C–H···Cl, π-stacking interactions as well as N–H···O, C–H···O and C–H···π hydrogen bonding interactions are involved in stabilizing the molecular self-association of the compounds. The theoretical study of the enclathration of the H-bonded 2-ClBzH dimer within a supramolecular cavity created by two [$Mn(phen)_2Cl_2$] complexes has been analyzed. This investigation utilized density functional theory (DFT) calculations, the non-covalent interaction (NCI) plot index, and the quantum theory of atoms in

 doi:10.20944/preprints202404.1039.v1

molecules (QTAIM) as computational methodologies. Additionally, molecular electrostatic potential (MEP) surface analysis was employed to examine synergistic effects.

2. Results and Discussion

2.1. Syntheses and General Aspects

$[Mn(phen)_2Cl_2]$2-ClBzH (**1**) has been synthesized by reacting one equivalent of $MnCl_2{\cdot}4H_2O$, one equivalent of 2-ClBzH and two equivalents of phen at room temperature in water medium. Similarly, $[Zn(4\text{-}MeBz)_2(2\text{-}AmPy)_2]$ (**2**) has been prepared by the reaction between one equivalent of $ZnCl_2$, two equivalents of Na-4-MeBzH and two equivalents of 2-AmPy at room temperature in water medium. The compounds are fairly soluble in water as well as in common organic solvents. Compound **1** shows room temperature (298 K) μ_{eff} value of 5.89 BM; which suggests the presence of five unpaired electrons in the Mn(II) centre of the distorted octahedral coordination sphere of **1** [56,57].

2.2. Crystal Structure Analysis

The molecular structure of compound **1** is shown in Figure 1. Selected bond lengths and bond angles around the Mn(II) centers have been summarized in Table 1. Compound **1** crystallizes in triclinic crystal system having $P\bar{1}$ space group. As shown in Figure 1, compound **1** is a mononuclear compound of Mn(II) which is hexa-coordinated with two bidentate phen moieties and two monodentate chloride ions. In addition; one uncoordinated 2-ClBzH moiety is also present in the crystal lattice. The coordination geometry around the Mn1 centre is distorted octahedron where the axial sites are occupied by N10A of phen and Cl1 atoms; whereas, the equatorial sites are occupied by N10B, N1B and N1A from phen moieties and Cl2 atoms. The four equatorial atoms viz. N10B, N1B, N1A, Cl2 are distorted from the mean equatorial plane with the mean r.m.s. deviation of 0.1712 Å. The dihedral angle between the two phen moieties is found to be 85.78°. The average Mn–N and Mn–Cl bond lengths are almost consistent with the previously reported Mn(II) complexes [58,59].

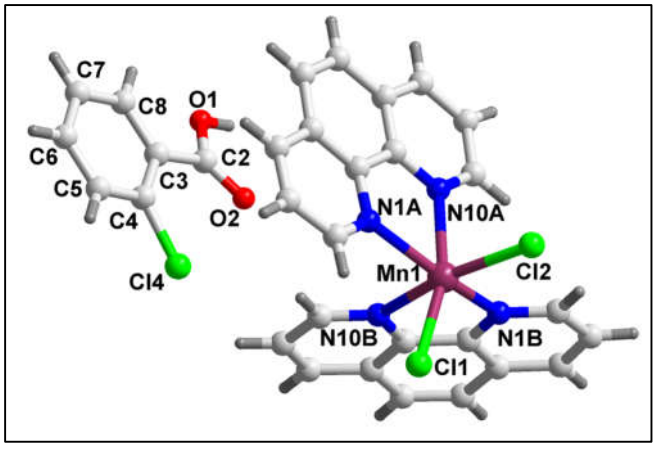

Figure 1. Molecular structure of $[Mn(phen)_2Cl_2]$2-ClBzH (**1**).

Table 1. Selected bond lengths (Å) and bond angles (°) of Mn(II) and Zn(II) centers in **1** and **2** respectively.

Bond lengths of **1** (Å)		Bond angles of **1** (°)	
Mn1–Cl1	2.4485(11)	N1A–Mn1–N1B	152.42(12)
Mn1–Cl2	2.4424(11)	N1A–Mn1–N10B	90.11(12)
Mn1–N1A	2.261(4)	N1B–Mn1–N10B	72.12(12)

 doi:10.20944/preprints202404.1039.v1

Mn1–N10A	2.343(4)	N1A–Mn1–N10A	71.99(13)
Mn1–N1B	2.284(3)	N1B–Mn1–N10A	85.34(12)
Mn1–N10B	2.320(3)	N10B–Mn1–N10A	85.22(12)
		N10A–Mn1–Cl1	104.06(9)
		N1A–Mn1–Cl2	92.28(8)
		N1B–Mn1–Cl2	164.38(9)
		N10B–Mn1–Cl2	92.87(9)
		N10A–Mn1–Cl2	94.5(1)
		N1A–Mn1–Cl1	105.22(9)
		N10B–Mn1–Cl1	87.27(9)
		N10A–Mn1–Cl1	164.49(9)
		Cl2–Mn1–Cl1	97.94(4)

Bond lengths of **2** (Å)		Bond angles of **2**(°)	
Zn1–O3	2.016(2)	O3–Zn1–N1	106.26(9)
Zn1–N1	2.070(3)	O3–Zn1–N3	96.24(9)
Zn1–N3	2.071(2)	N1–Zn1–N3	104.32(10)
Zn1–O1	2.105(3)	O3–Zn1–O2	92.21(9)
Zn1–O2	2.292(3)	N1–Zn1–O2	143.86(11)
Zn1–C1	2.535(3)	N3–Zn1–O2	104.17(9)
O1–Zn1–O2		59.39(10)	
		O3–Zn1–O1	149.88(11)
		N1–Zn1–O1	93.92(10)
		N3–Zn1–O1	100.20(11)

The monomeric units of compound **1** are interconnected via weak C–H···Cl hydrogen bonding and aromatic π-stacking interactions that are responsible for the formation of the 1D supramolecular chain of the compound (Figure 2). Cl1 atom is involved in two C–H···Cl hydrogen bonding interactions with the –CH moieties of phen having C8B–H8B···Cl1 and C4B–H4B···Cl1 distances of 2.75 and 2.81 Å respectively. Moreover, aromatic π-stacking interactions are also observed between the aromatic rings of phen with centroid(N1B, C2B, C3B, C4B, C12B and C11B)-centroid(N1B, C2B, C3B, C4B, C12B and C11B) separation of 3.49 Å. The ring normal and the vector between the two ring centroids form an angle (slipped angle) of about 22.28° which is close to the slipped π-stacking interactions reported in the literature [60].

Uncoordinated 2-ClBzH molecules of compound **1** form a hydrogen bonded supramolecular dimer assisted by strong O–H···O hydrogen bonding interactions (Figure 3). O–H···O hydrogen bonding interactions between the two 2-ClBzH moieties is observed having O1–H1···O2

 doi:10.20944/preprints202404.1039.v1

distance of 1.79 Å. The supramolecular ring motif formed in the cyclic supramolecular dimer has been expressed using Etter's graph-set notation [61] viz. $R_2^2(8)$.

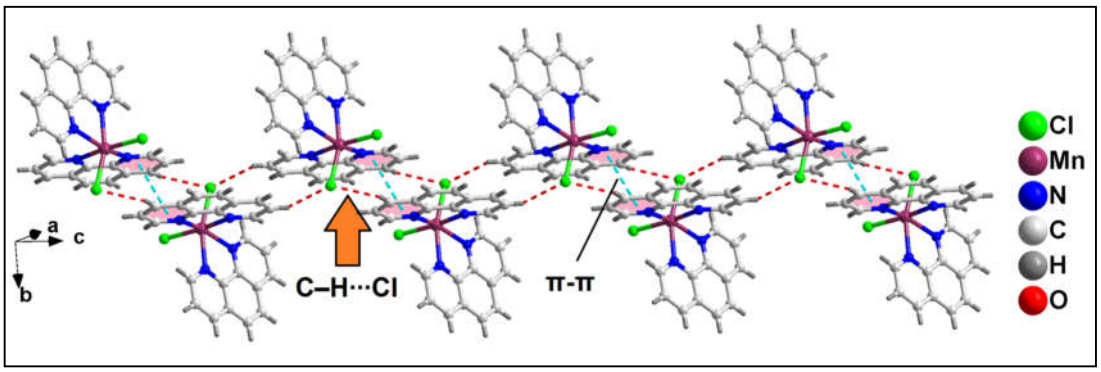

Figure 2. 1D supramolecular chain of compound **1** along the crystallographic c axis assisted by C–H···Cl and π-stacking interactions.

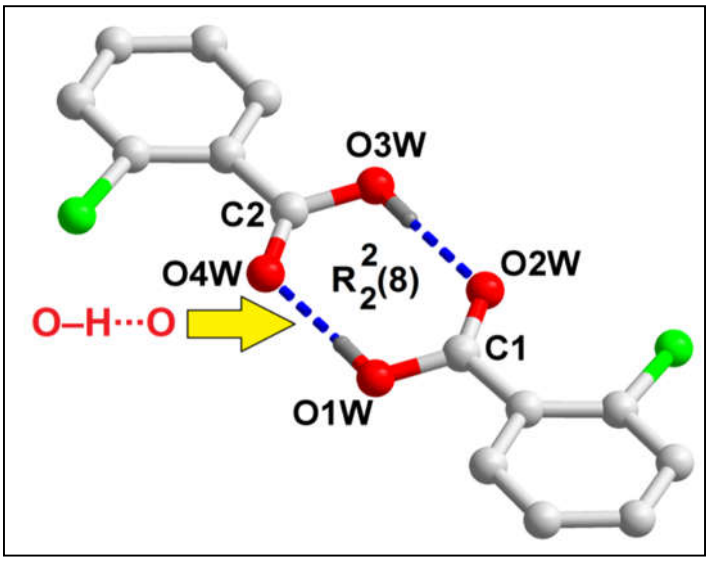

Figure 3. Formation of supramolecular dimer of 2-ClBzH in compound **1** assisted by O–H···O hydrogen bonding interactions. Aromatic hydrogen atoms have been omitted for clarity.

The supramolecular dimer is enclathrated within the supramolecular host cavity formed by six different monomeric units assisted by the weak C–H···Cl contacts (Figure 4). In addition, O-π contacts are observed involving the pyridine rings of the phen moieties having O1-Cg (Cg is the centroid of the ring formed by the atoms N10B, C9B, C8B, C7B, C14B and C13B) and O2-Cg distances of 3.91 Å and 3.18 Å respectively. Cl-π contacts are also observed involving the pyridine rings of the phen moieties having Cl4-Cg_1 (Cg_1 is the centroid of the ring formed by the atoms C12A, C11A, N1A, C2A, C3A and C4A) distance of 3.92 Å. These enclathrated dimers of 2-ClBzH propagate along the crystallographic bc plane to stabilize the layered architecture of the compound (Figure 5).

Further analysis reveals that C–H···Cl hydrogen bonding interactions play a crucial role in the propagation of the supramolecular 1D chains to form the layered architecture. Along the crystallographic ab plane, two types of C–H···Cl hydrogen bonding interactions are observed between the neighboring monomeric units (Figure 6). Cl2 atom is involved in a C–H···Cl interaction with the pyridyl ring of phen moiety, having a C7B–H7B···Cl2 distance of 2.92 Å; while Cl1 atom is also involved in C–H···Cl interaction with the pyridyl ring of phen moiety, having a C4B–H4B···Cl1 distance of 2.81 Å.

 doi:10.20944/preprints202404.1039.v1

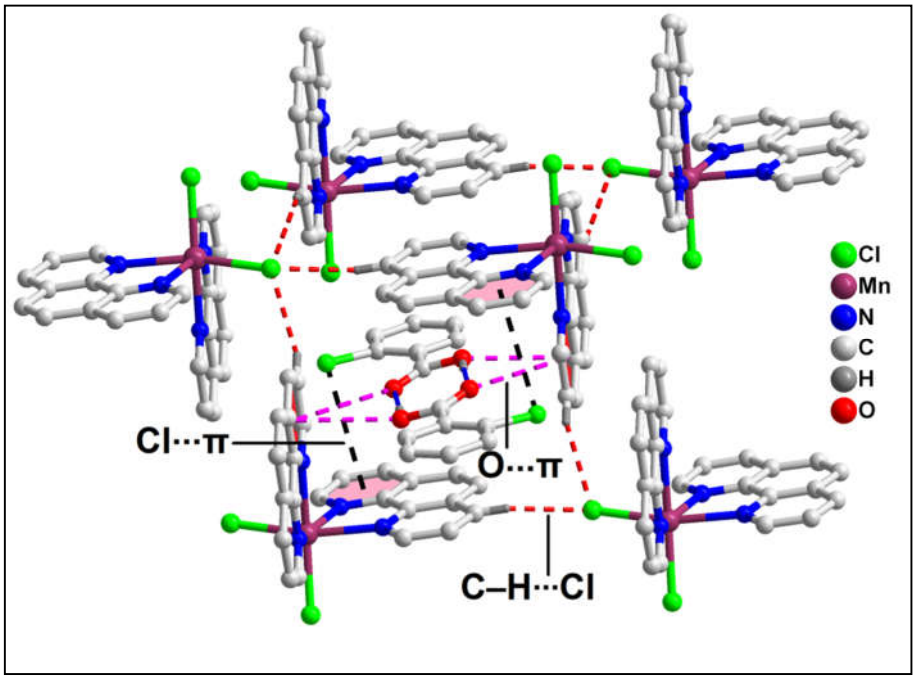

Figure 4. Enclathration of the hydrogen bonded dimer of 2-ClBzH inside the supramolecular hexameric host cavity of **1**.

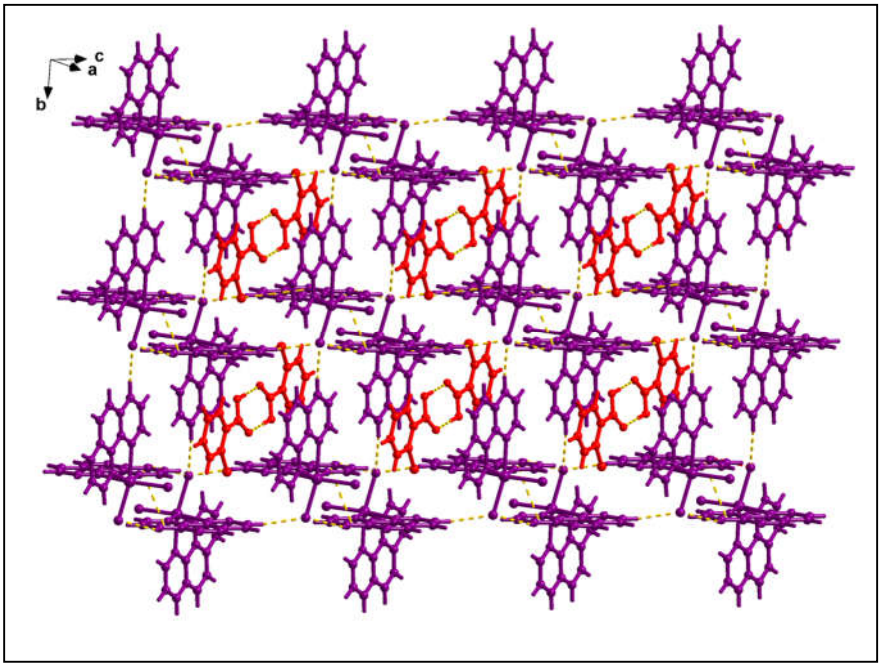

Figure 5. Layered assembly of compound **1** along the crystallographic bc plane.

 doi:10.20944/preprints202404.1039.v1

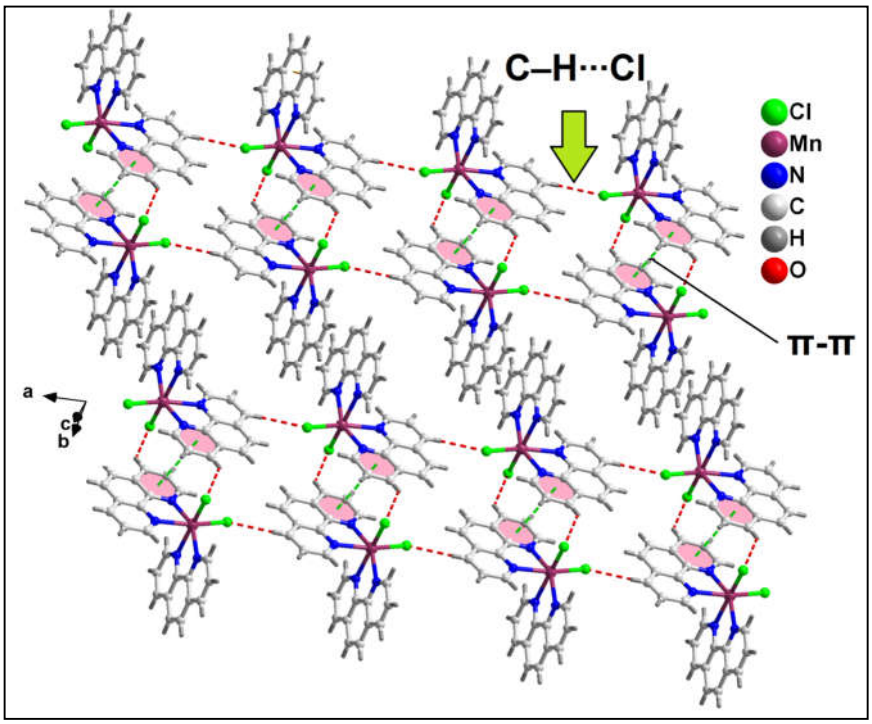

Figure 6. Layered assembly of compound **1** along the crystallographic ab plane.

Table 2. Selected hydrogen bond distances (Å) and angles (deg.) for compound **1.**

D–H···A	d(D···A)	d(H···A)	<(DHA)
C7B–H7B···Cl2	3.701	2.92	139.3
O1–H1···O2	2.635	1.79	177.2
C8B–H8B···Cl1	3.566	2.75	144.3
C4B–H4B···Cl1	3.502	2.81	130.4

The molecular structure of compound **2** is shown in Figure 7. Selected bond lengths and bond angles around the Zn(II) centers have been summarized in Table 1. Compound **2** crystallizes in monoclinic crystal system having Cc space group. As shown in Figure 7, compound **2** comprises of a mononuclear Zn(II) metal centre. Zn1 centre in compound **2** is penta-coordinated with two monodentate 2-AmPy moieties, one monodentate 4-MeBz moiety and one bidentate 4-MeBz moiety. The coordination geometry around Zn1 centre is distorted square pyramidal (evidenced by the value of the trigonality index $\tau = 0.1003$) where the axial site is occupied by N3 atom; whereas the equatorial sites are occupied by O2, O3 and O1 atoms from two 4-MeBz moieties and N1 atom from one 2-AmPy moiety. The equatorial atoms viz. O1, O2, O3 and N1 of the Zn1 centre are distorted from the mean equatorial plane with the mean r.m.s. deviation of 0.1120 Å. The average Zn–O and Zn–N bond lengths are almost consistent with the previously reported Zn(II) complexes [62].

The neighboring complex moieties in compound **2** are interconnected via N–H···O and C–H···O hydrogen bonding interactions with N2–H2B···O2 distance of 2.03 Å and C19–H19···O2, C20–H20···O4 distances of 2.80 Å and 2.58 Å respectively to form the 1D supramolecular chain along the crystallographic a axis (Figure 8). Moreover C–H···π in teractions are also observed in the 1D supramolecular chain involving the –CH moieties of 4-MeBz and 2-AmPy and ring centroid of 4-MeBz with H6···Cg_2, C6···Cg_2 (Cg_2 is the ring centroid defined by the atoms C10-C15) and H23···Cg_2, C23···Cg_2 distances of 2.73, 3.66 and 2.63, 3.52 Å respectively provide extra ballast to the propagation

 doi:10.20944/preprints202404.1039.v1

of the 1D chain along the crystallographic a axis. The C6–H6···Cg_2 and C23–H23···Cg_2 bond angles observed are 165.60° and 156.18° respectively.

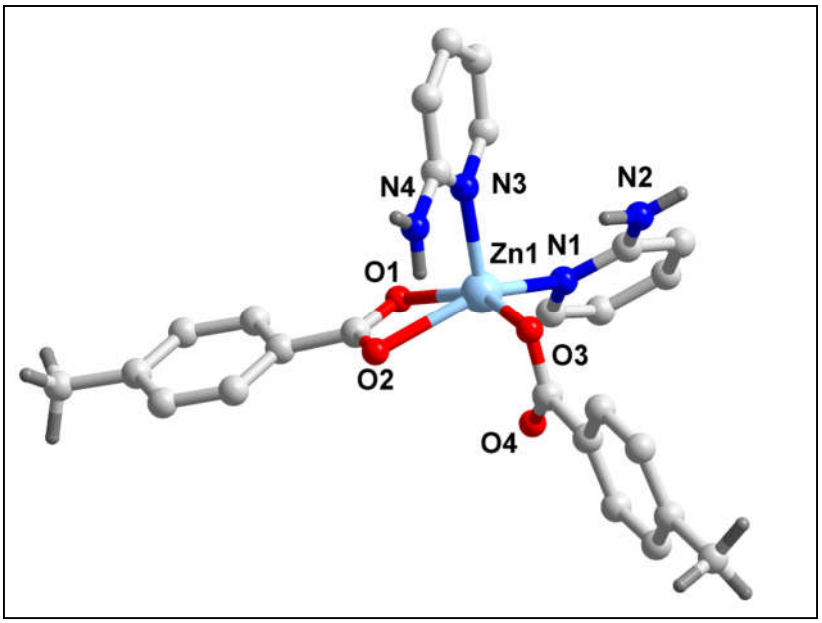

Figure 7. Molecular structure of [Zn(4-MeBz)$_2$(2-AmPy)$_2$] (**2**). Aromatic hydrogen atoms have been omitted for clarity.

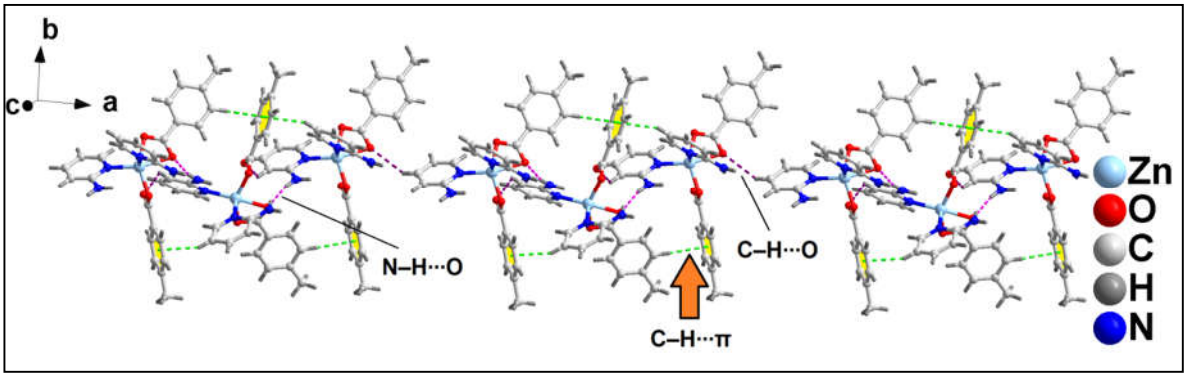

Figure 8. 1D supramolecular chain of the compound **2** along the crystallographic a axis assisted by C–H···O, N–H···O hydrogen bonding and non-covalent C–H···π interactions.

The 1D supramolecular chains are interconnected via C–H···O hydrogen bonding interactions to form the layered assembly along the crystallographic ab plane (Figure 9). The C–H···O hydrogen bonding interactions is formed between the –C16H16B moiety of 4-MeBz with the O1 atom of another 4-MeBz of adjacent monomeric chain having C16–H16B···O1 distance of 2.68 Å.

Further analysis reveals the presence of C–H···π and C–H···O hydrogen bonding interactions that play pivotal role for the formation of layered assembly of compound **2** along the crystallographic ac plane (Figure 10). C–H···O hydrogen bonding interaction is formed between the –CH moiety and O2 atom of 4-MeBz having C19–H19···O2 distance of 2.80 Å. C–H···π interaction is also observed between the –C24H24 moiety of 2-Ampy and aromatic ring of 4-MeBz with H24···Cg_3 and C24···Cg_3 (Cg_3 is the ring centroid defined by the atoms C2-C7) distances of 2.62 and 3.54 Å respectively. The C24–H24···Cg_3 bond angle observed is 160.97°.

 doi:10.20944/preprints202404.1039.v1

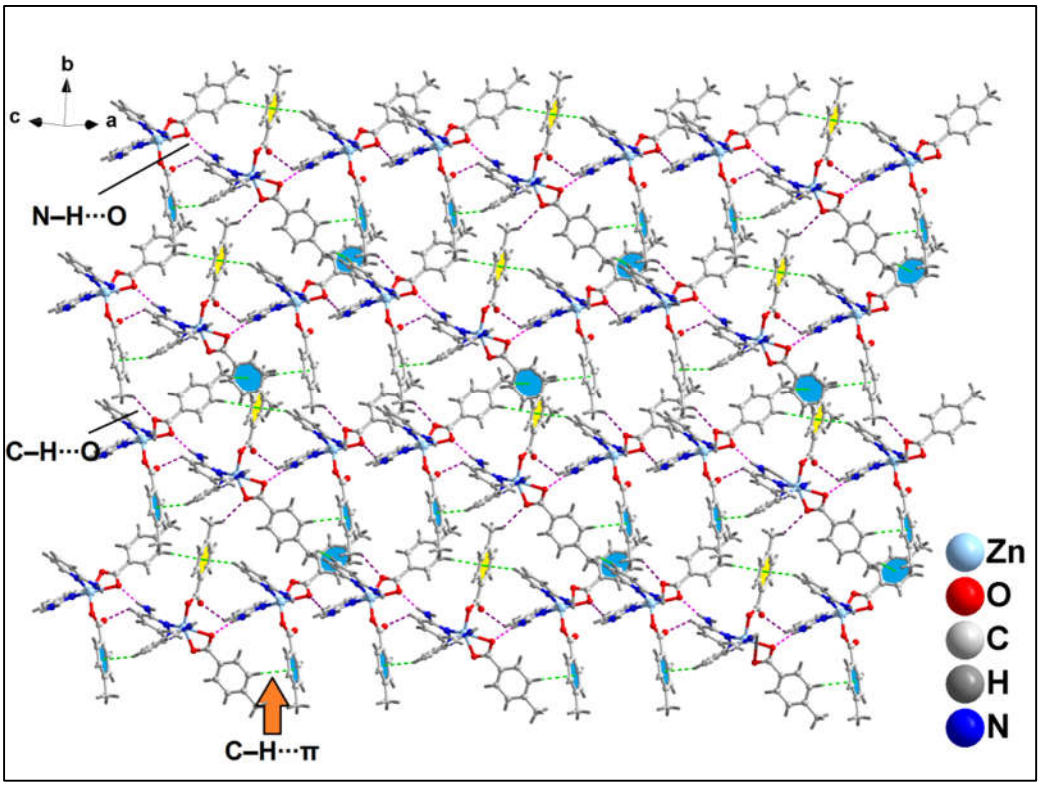

Figure 9. Layered assembly of compound **2** along the crystallographic ab plane.

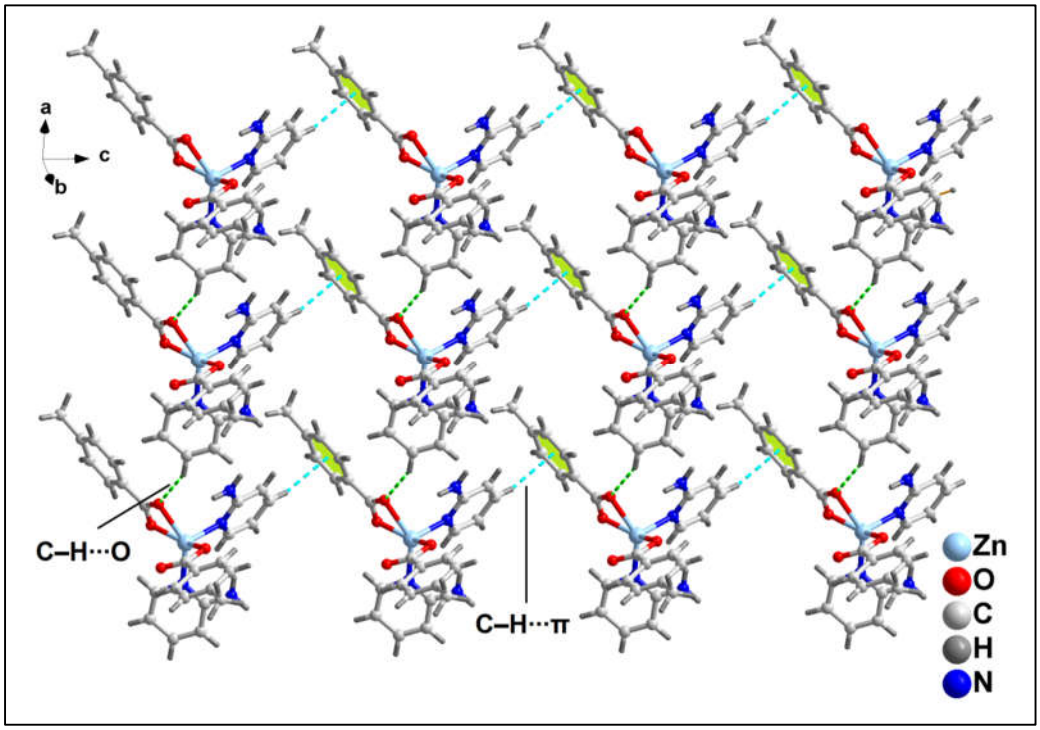

Figure 10. Layered assembly of compound **2** along the crystallographic ac plane.

Table 3. Selected hydrogen bond distances (Å) and angles (deg.) for compound **2.**

D–H···A	d(D···A)	d(H···A)	<(DHA)
N2–H2B···O2	2.906	2.03	168.435

 doi:10.20944/preprints202404.1039.v1

C19–H19···O2	3.623	2.80	145.031
C20–H20···O4	3.197	2.58	122.597
C16–H16B···O1	3.522	2.68	122.597

2.3. Spectral Studies

2.3.1. FT-IR Spectroscopy

The FT-IR spectra of compounds **1** and **2** have been recorded in the region 4000-500 cm^{-1} (Figure S1). The comparatively broad absorption bands in the FT-IR spectra of compound **1** at around 3411 cm^{-1} can be attributed to the O-H stretching vibrations of the carboxyl group of 2-ClBzH moiety present in the crystal lattice [63–65]. The ring stretching vibrations for 2-AmPy ligands have been shifted to lower wave numbers (1565, 1453, 1272 cm^{-1}) in the FT-IR spectrum of compound **2** suggesting the coordination of 2-AmPy with a Zn(II) centre via a pyridine ring N-atom [66,67]. The wagging vibrations of the pyridine rings are observed at 666 and 695 cm^{-1} [68]. The bands at 1610 and 1496 cm^{-1} in the FT-IR spectrum of **2** can be attributed to the asymmetric ν_{as}(COO) and symmetric ν_{s}(COO) stretching vibrations of the carboxylate moiety of coordinated 4-MeBz. The difference between asymmetric and symmetric stretching vibrations of the carboxylate moieties ($\Delta < 200$ cm^{-1}) indicates the bidentate coordination of carboxylate to the respective metal center in compound **2** [69,70]. The absence of any bands near 1710 cm^{-1} in compound **2** indicates deprotonation of carboxylate groups of the compound [71]. Weak absorptions observed around 2730-3070 cm^{-1} can be attributed to the ν(C–H) vibrations of the 4-Mebz moieties [72]. In compound **1**, the coordination of phen to the metal centers can be confirmed by the shifting of IR frequencies for δ(C-H) vibrations of phen [73,74]. The bands around 1420 and 1151 cm^{-1} for compounds **1** and **2** can be attributed to the ν(C=C) and ν(C=N) vibrations of coordinated phen [75].

2.3.2. Electronic Spectroscopy

The electronic spectra of the compounds have been recorded in both solid and aqueous phases (Figure S2 and S3). The spectra of the compounds reveal the presence of Mn(II) and Zn(II) centers in the compounds **1** and **2** respectively [76–82]. The absorption peaks for the $\pi \rightarrow \pi^*$ transition of the aromatic ligands are obtained at the expected positions [83,84].

2.4. Thermogravimetric Analysis

Thermogravimetric curves of the compounds **1** and **2** were obtained in the temperature range 25-1000°C at the heating rate of 10°C/min under N_2 atmosphere (Figure S4). For compound **1**; in the temperature range 230-390°C, 2-ClBzH moiety present in the lattice and one coordinated phen moiety are decomposed with the observed weight loss of 47.50% (calcd. = 52.35%) [85,86]. In the temperature range 391-520°C, decomposition of another coordinated phen moiety with the weight loss of 29.20% (calcd. = 28%) [86] is observed. In the final step, loss of one coordinated Cl ion in the temperature range 521-960°C is observed with weight loss of 7% (calcd = 5.52%) [87]. For compound **2**; in the temperature range 180-273°C, two coordinated 2-AmPy moieties undergo thermal decomposition with the observed weight loss of 37.66% (calcd. = 35.88%) [88]. One coordinated 4-MeBz moiety and a $–CO_2$ and $–CH_3$ fragments from the other coordinated 4-MeBz moiety undergo decomposition in the temperature range 274-650°C with the observed weight loss of 37.64% (calcd. 37.02%) [89].

2.5. Theoretical Study

This theoretical investigation deals with the enclathration of the H-bonded 2-ClBzH dimer within the supramolecular host cavity formed by complex molecules viz. $[Mn(phen)_2Cl_2]$. The study commenced with the calculation of the molecular electrostatic potential (MEP) surfaces for both $[Mn(phen)_2Cl_2]$ and 2-ClBzH co-formers, to pinpoint their nucleophilic and electrophilic regions. The

 doi:10.20944/preprints202404.1039.v1

MEP analysis of [Mn(phen)$_2$Cl$_2$] (Figure 11a) reveals the presence of nucleophilic zones at the chlorido moieties (–72.5 kcal/mol) and electrophilic zones at the phen with the MEP maximum on the aromatic hydrogen atoms (+28.2 kcal/mol). This polarization correlates with the formation of a 2D layered structure along the ab crystallographic plane, dominated by CH···Cl interactions as shown in Figure 6. The MEP surface for the 2-ClBzH molecule (Figure 11b) displays an expected MEP maximum at the acidic hydrogen (+50 kcal/mol) and a minimum at the oxygen atom (–34.5 kcal/mol), with negative potentials also observed at the chlorine belt (–12.5 kcal/mol) and over the aromatic ring's center (–2.5 kcal/mol). Upon dimerization, the MEP landscape of 2-ClBzH transforms, with the maximum now over the aromatic hydrogen atoms (20.0 kcal/mol) and the minimum at the region influenced by oxygen and chlorine atoms (–28.2 kcal/mol, see Figure 11c), highlighting an electron-rich surface extending from the core of four oxygen atoms to the chlorine's belts and the π-basic aromatic rings, revealing a pronounced complementarity with the positive cleft of [Mn(phen)$_2$Cl$_2$].

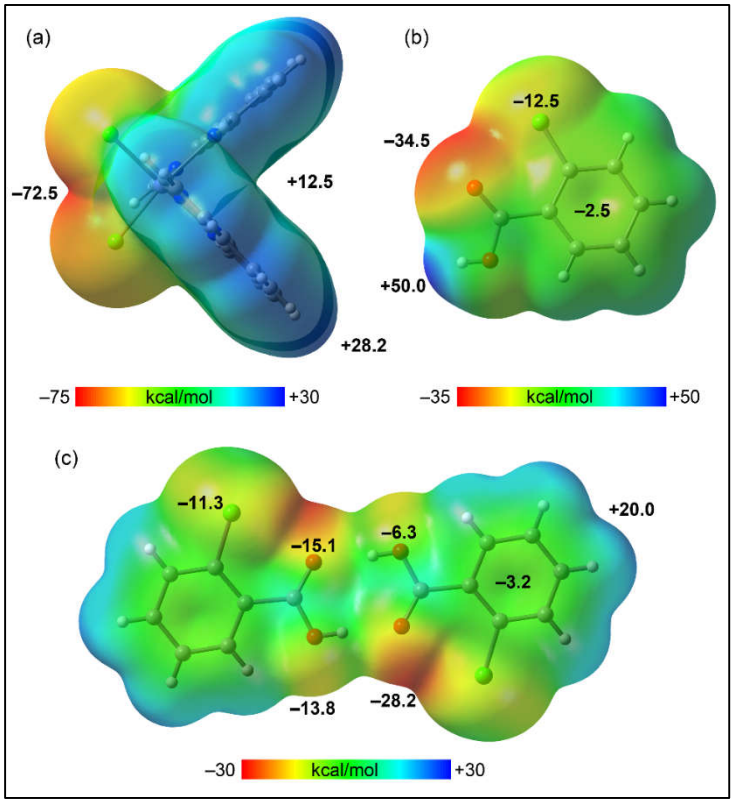

Figure 11. MEP surfaces of [Mn(phen)$_2$Cl$_2$] (a), 2-ClBzH (b) and its dimer (c), setting an isovalue of 0.001 a.u.

Figure 12a presents the QTAIM and NCI plot analysis for the 2-ClBzH dimer, showcasing bond critical points (BCPs), bond paths, and blue RDG isosurfaces for each OH···O bond, evidencing the strong nature of the H-bonds with a significant dimerization energy of –13.7 kcal/mol. This robustness explains the dimers' formation in the solid state. Further analysis of the dimer's interaction with two [Mn(phen)$_2$Cl$_2$] molecules to create a tetrameric assembly revealed a substantial interaction energy of –47.5 kcal/mol, driven by multiple cooperative interactions, predominantly analyzed through NCI Plot for clarity. The interactions involve CH···Cl and Cl···π(phen) interactions, highlighted by green RDG isosurfaces. Moreover, larger RDG isosurfaces are also observed between the oxygen atoms and the π-systems of phen ligands indicating the formation of O···π interactions in a T-shaped arrangement (outlined in Figure 12b using dashed rectangles). Additionally, extensive RDG isosurfaces above and below the 2-ClBzH dimer characterize the electrostatically enhanced π-stacking interactions that embrace two phen ligands (above and below the dimer) and the entire 2-ClBzH dimer including the aromatic rings and the supramolecular $R_2^2(8)$. ring. This complex interplay of forces explains the significant formation energy and suggests that the formation of the

Preprints.org (www.preprints.org) | NOT PEER-REVIEWED | Posted: 16 April 2024 doi:10.20944/preprints202404.1039.v1

H-bonded dimer notably increases its potential for interaction with [Mn(phen)$_2$Cl$_2$], promoting its enclathration.

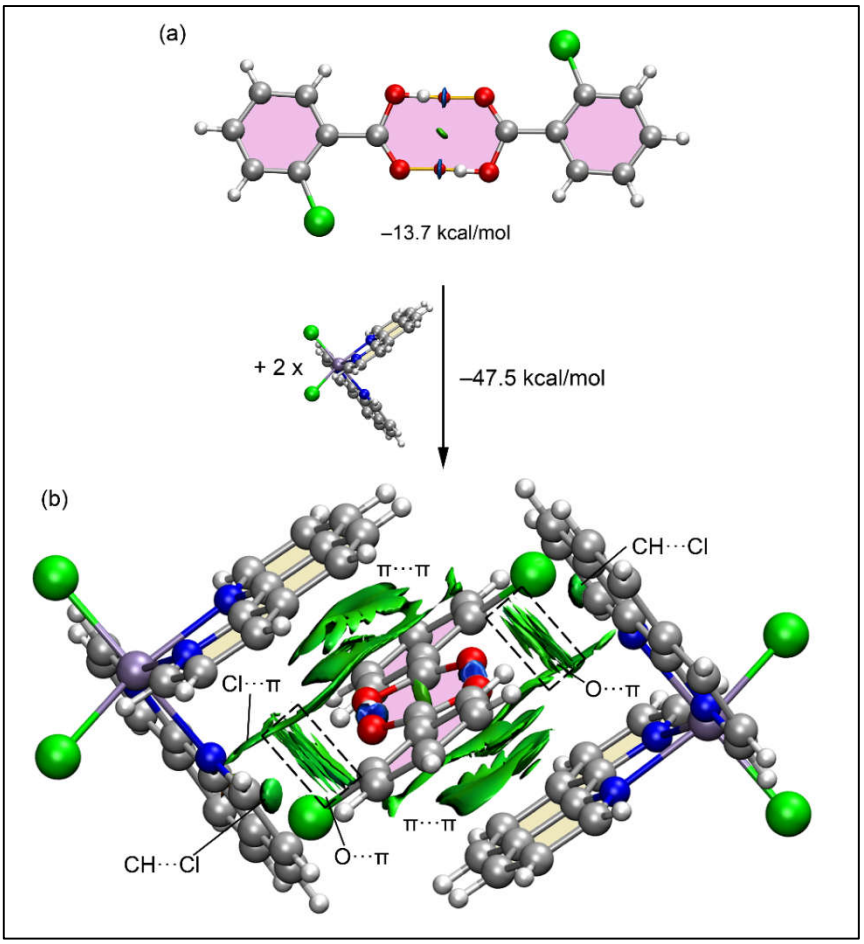

Figure 12. (a) QTAIM and NCIplot analysis of the self-assembled dimer of 2-ClBzH and the dimerization energy. (b) NCIplot analysis of the tetrameric assembly and the formation energy starting from the dimer and two molecules of [Mn(phen)$_2$Cl$_2$]. Only intermolecular interactions are shown.

3. Materials and Methods

All chemicals viz. manganese(II) chloride tetrahydrate, anhydrous zinc(II) chloride, 2-aminopyridine, 2-chlorobenzoic acid, 4-methylbenzoic acid and 1,10-phenanthroline used for synthesis were obtained from commercial sources and were used as received. Elemental analyses (C, H and N) was carried out using Perkin Elmer 2400 series II CHNS/O analyzer. IR spectra were as KBr pellets with Bruker Alpha (II) infrared spectrophotometer from 4000-500 cm^{-1}. The diffuse-reflectance UV-Vis spectra were obtained using a Shimadzu UV-2600 spectrophotometer. BaSO4 powder was employed as a reference to establish 100% reflectance for solid-state UV-Vis NIR spectra. Room temperature magnetic susceptibilities were assessed at 300 K using the Evans method on the Sherwood Mark 1 Magnetic Susceptibility balance. Thermogravimetric analysis were carried in the 25-500 °C range (at the heating rate of 10°C min^{-1}) under a N_2 atmosphere on a Mettler Toledo TGA/DSC1 STAR^e system.

3.1. Syntheses

3.1.1. Synthesis of [Mn(phen)$_2$Cl$_2$]2-ClBzH (1)

The Mn(II) complex was prepared by dissolving 0.360 g (2 mmol) of Phen in 10 mL of de-ionised water in a round bottom flask, to which an aqueous solution (5 ml) 0f 0.197 g (1 mmol) of $MnCl_2{\cdot}4H_2O$

Preprints.org (www.preprints.org) | NOT PEER-REVIEWED | Posted: 16 April 2024 doi:10.20944/preprints202404.1039.v1

was added with continuous stirring then left at room temperature for about an hour. To the resulting solution, an aqueous solution (5 ml) of 0.156 g (1 mmol) of 2-chlorobenzoic acid was added slowly and the mixture was kept under mechanical stirring for another hour (Scheme 1). The resulting solution was left undisturbed in cooling conditions (2-4°C) ; and yellow block shaped crystals were obtained after a few days. Yield: 0.520 g (81.12%). Anal. calcd. for $C_{31}H_{21}Cl_3MnN_4O_2$: C, 57.92%; H, 3.29%; N, 8.72%; Found: C, 57.82%; H, 3.18%; N, 8.60%. FT-IR (KBr pellet, cm^{-1}): 3411(br), 3063(w), 2668(w), 2550(w), 1690(s), 1605(m), 1524(s), 1420(s), 1334(m), 1296(s), 1151(w), 1123(sh), 1105(w), 931(w), 857(w), 791(w), 716(w) (s, strong; m, medium; w, weak; br, broad; sh, shoulder).

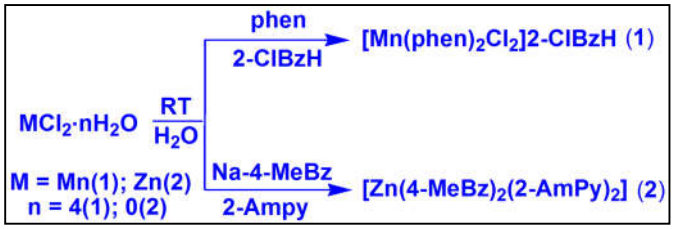

Scheme 1. Syntheses of the compounds **1** and **2**.

3.1.2. Synthesis of $[Zn(4\text{-}MeBz)_2(2\text{-}AmPy)_2]$ (2)

Zinc(II) chloride 0.136 g (1 mmol) was dissolved in 5 ml of de-ionised water, to which an aqueous solution (5 ml) of 0.316 g (2 mmol) of sodium salt of 4-methylbenzoic acid was added drop by drop with continuous stirring for an hour. After 1 hour, an aqueous solution (5 ml) of 0.188 g (2 mmol) of 2-AmPy was added to the solution and left for stirring for another one hour (Scheme 1). The resulting solution was left undisturbed in a refrigerator below 4°C for crystallization; from which colourless prism shaped crystals suitable for single crystal X-ray diffraction were obtained after few days. Yield: 0.468 g (89.56%). Anal. calcd. For $C_{26}H_{26}N_4O_4Zn$: C, 59.61%; H, 5.00%; N, 10.69%; Found: C, 59.55%; H, 4.95%; N, 10.60%. FT-IR (KBr pellet, cm-1): 3338(br), 2729(w), 2925(w), 1645(s), 1610(s), 1566(s), 1496(s), 1453(s), 1439(m), 1272(m), 1163(w), 1151(w), 1096(w), 1009(w), 860(w), 790(w), 770(w), 741(w), 695(w), 666(m) (s, strong; m, medium; w, weak; br, broad; sh, shoulder).

3.2. Crystallographic Data Collection and Refinement

The single crystal XRD data of compound 1 and 2 collections were acquired employing a Bruker D8 Venture diffractometer (Karlsruhe, Germany) equipped with a Photon III 14 detector, and utilizing an Incoatec high brilliance I S DIAMOND tube [Cu/Kα radiation (λ = 1.54178 Å)], along with an Incoatec Helios MX multilayer optics. The data collection was performed at 100 K for the crystals. Scaling and absorption corrections were performed using the SADABS program for all datasets [90]. Crystal structures were solved by direct method and refined on F^2 by full matrix least squares technique with SHELXL-2018/3 [91] using the WinGX [92] platforms. Non-hydrogen atoms were refined with anisotropic thermal parameters. The hydrogen atoms of the organic ligands were placed in ideal positions and refined as riding atoms. Diamond 3.2 software is used for graphical illustrations [93]. Crystallographic data of the compounds **1** and **2** have been summarized in Table 4 and CCDC deposition numbers have been cited in Appendix A.

Table 4. Crystallographic data and structure refinement details for **1** and **2.**

Parameters	**1**	**2**
Formula	$C_{31}H_{21}Cl_3MnN_4O_2$	$C_{26}H_{26}N_4O_4Zn$
Formula weight	642.81	523.88
Temp, [K]	100	100

 doi:10.20944/preprints202404.1039.v1

Crystal system	Triclinic	Monoclinic
Space group	$P\bar{1}$	Cc
a, [Å]	10.6563(18)	9.9347(14)
b, [Å]	10.9066(19)	23.521(3)
c, [Å]	12.790(2)	10.5889(15)
α, [°]	89.159(9)	90
β, [°]	66.391(7)	93.195(4)
γ, [°]	86.483(8)	90
V, [Å^3]	1359.4(4)	2470.5(6)
Z	2	4
Absorption coefficient (mm^{-1})	6.977	1.709
F(0 0 0)	654.0	1088.0
ϱ_{calc}g/cm^3	1.570	1.409
index ranges	-12 ≤ h ≤ 12, -12 ≤ k ≤ 13, -15 ≤ l ≤ 15	-11 ≤ h ≤ 11, -28 ≤ k ≤ 28, -12 ≤ l ≤ 12
Crystal size, [mm^3]	0.38 × 0.28 × 0.25	0.38 × 0.31 × 0.15
2θ range, [°]	8.122 to 137.828	9.676 to 136.904
Independent Reflections	4832	4216
Reflections collected	53812	26679
Refinement method	Full-matrix least-squares on F^2	Full-matrix least-squares on F^2
Data/restraints/ parameters	4832/0/371	4216/2/319
Goodness-of-fit on F^2	1.060	0.831
Final R indices [I > 2σ(I)]	R_1 = 0.0773, wR_2 = 0.2158	R_1 = 0.0281, wR_2 = 0.0725
R indices (all data)	R_1 = 0.0812, wR_2 = 0.2233	R_1 = 0.0281, wR_2 = 0.0725
Largest hole and peak [e·Å^{-3}]	1.00/-1.06	0.73/-0.37

3.3. Computational Methods

Single-point calculations were conducted using the Turbomole 7.7 program [94] at the RI-BP86-D4/def2-TZVP level of theory [95–97]. Crystallographic coordinates were utilized to evaluate

 doi:10.20944/preprints202404.1039.v1

noncovalent interactions within compound 1, to evaluate the interactions as they stand in the solid state. To analyze these interactions, Bader's "Atoms in molecules" theory (QTAIM) [98] and the non-covalent interaction plot (NCI plot) [99] were employed via the Multiwfn program [100], with visualizations generated using VMD visualization software version 1.9 [101]. The binding energies were calculated using a supramolecular approach, subtracting the sum of the energies of the monomers from the energy of the assembled complex. The molecular electrostatic potential (MEP) surface was represented at an isosurface of 0.001 a.u., reflecting the van der Waals surface.

4. Conclusions

Two new Mn(II) and Zn(II) metal-organic compounds involving 1,10-phenanthroline and methyl-benzoate have been synthesized and characterized using single crystal X-ray diffraction, electronic, FT-IR, and TGA analyses. Crystal structure analysis of compound **1** revealed the dimerization of 2-ClBzH moieties present in the lattice and their subsequent enclathration within the hexameric supramolecular host cavity formed by the orderly monomeric units. Similarly crystal structure analysis of compound **2** unfolded the dual mode of coordination of 4-CH_3Bz with the metal centre and their role in the self-aggregation of the individual units towards the formation of novel supramolecular architectures. Moreover non-covalent interactions involving lp(O)-π, lp(Cl)-π, C–H···Cl, π-stacking interactions as well as N–H···O, C–H···O and C–H···π hydrogen bonding interactions are found to be involved in stabilizing the molecular self-association of the compounds. The theoretical investigation provides some insights into the mechanism of supramolecular assembly in compound **1**. MEP surface analysis of 2-ClBzH dimer in **1** reveals the existence of electron-rich surface encompassing the oxygen, chlorine and π-basic atoms of aromatic ring suggesting symbiosis with the positive cleft of [$Mn(phen)_2Cl_2$]. Further energetically significant dimerization energy of 2-ClBzH and substantial interaction energy of the dimer with [$Mn(phen)_2Cl_2$] molecules suggest formation of the dimer, its enclathration within the hexameric host and the cooperative nature of multiple non-covalent interactions. These findings enrich our understanding of the principles governing the design and stabilization of complex supramolecular structures, potentially guiding future research and applications in materials science and molecular engineering.

Supplementary Materials: The following supporting information can be downloaded at the website of this paper posted on Preprints.org. Figure S1: FT-IR spectra of compounds **1** and **2**; Figure S2: (a) UV-Vis-NIR spectrum of **1**, (b) UV-Vis spectrum of **1**; Figure S3: (a) UV-Vis-NIR spectrum of **2**, (b) UV-Vis spectrum of **2**; Figure S4: Thermogravimetric curves of the compounds **1** and **2**.

Author Contributions: Conceptualization, A.F. and M.K.B.; methodology, A.F. and M.K.B.; software, A.F. and R.M.G.; formal analysis, A.F.; investigation, M.B.; S.B. and R.M.G.; data curation, M.B.-O.; writing—original draft preparation, M.B.; writing—review and editing, M.K.B.; visualization, A.F.; supervision, M.K.B.; project administration, A.F. and M.K.B.; funding acquisition, A.F. and M.K.B. All authors have read and agreed to the published version of the manuscript.

Funding: Financial support was provided by SERB-SURE (Grant number: SUR/2022/001262); ASTEC, DST, Govt. of Assam (grant number ASTEC/S&T/192(177)/2020-2021/43) and the Gobierno de Espana, MICIU/AEI (project number PID2020-115637GB-I00) and Department of Biotechnology (DBT), Government of India (Project No. BT/INF/22/SP45376/2022), all of whom are gratefully acknowledged. The authors thank IIT-Guwahati for the TG data.

Data Availability Statement: Data are contained within the article and Supplementary Materials.

Conflicts of Interest: The authors declare no conflict of interest. The funders had no role in the design of the study; in the collection, analyses, or interpretation of data; in the writing of the manuscript; or in the decision to publish the results.

Appendix A

CCDC 2322621 and 2322622 contains the supplementary crystallographic data for the compounds **1** and **2**. These data can be obtained free of charge at http://www.ccdc.cam.ac.uk or from the Cambridge Crystallographic Data Centre, 12 Union Road, Cambridge CB2 1EZ, UK; fax: (+44) 1223-336-033; or E-mail: deposit@ccdc.cam.ac.uk.

 doi:10.20944/preprints202404.1039.v1

References

1. Wang, H. S.; Wang, Y. H.; Ding, Y. Development of Biological Metal–Organic Frameworks Designed for Biomedical Applications: From Bio-Sensing/Bio-Imaging to Disease Treatment. *Nanoscale Adv.* **2020**, *2*, 3788–3797.
2. Bavykina, A.; Kolobov, N.; Khan, I. S.; Bau, J. A.; Ramirez, A.; Gascon, J. Metal–Organic Frameworks in Heterogeneous Catalysis: Recent Progress, New Trends, and Future Perspectives. *Chem. Rev.* **2020**, *120*, 8468–8535.
3. Lian, H.; Cheng, X.; Hao, H.; Han, J.; Lau, M.-T.; Li, Z.; Zhou, Z.; Dong, Q.; Wong, W.-Y. Metal-Containing Organic Compounds for Memory and Data Storage Applications. *Chem. Soc. Rev.* **2022**, *51*, 1926–1982.
4. Gao, P.; Chen, Y.; Pan, W.; Li, N.; Liu, Z.; Tang, B. Antitumor Agents Based on Metal–Organic Frameworks. *Angew. Chem.* **2021**, *133*, 16901–16914.
5. Zheng, R.; Guo, J.; Cai, X.; Bin, L.; Lu, C.; Singh, A.; Liu, J. Manganese Complexes and Manganese-Based Metal-Organic Frameworks as Contrast Agents in MRI and Chemotherapeutics Agents: Applications and Prospects. *Colloids Surf., B* **2022**, *213*, 112432-112440.
6. Li, X.; Kang, Q.; Liu, L.; Ma, J.; Dong, W. Trinuclear Co(II) and Mononuclear Ni(II) Salamo-Type Bisoxime Coordination Compounds. *Crystals* **2018**, *8*, 43-60.
7. Gu, J.; Wen, M.; Cai, Y.; Shi, Z.; Nesterov, D. S.; Kirillova, M. V.; Kirillov, A. M. Cobalt(II) Coordination Polymers Assembled from Unexplored Pyridine-Carboxylic Acids: Structural Diversity and Catalytic Oxidation of Alcohols. *Inorg. Chem.* **2019**, *58*, 5875–5885.
8. Tang, L.; Tang, L.; Wang, D.; Deng, H.; Chen, K. Metal and Ligand Effects on the Stability and Electronic Properties of Crystalline Two-Dimensional Metal-Benzenehexathiolate Coordination Compounds. *J. Phys. Condens. Matter* **2018**, *30*, 465301–465306.
9. Abdel-Rahman, L. H.; Abdelhamid, A. A.; Abu-Dief, A. M.; Shehata, M. R.; Bakheeta, M. A. Facile Synthesis, X-Ray Structure of New Multi-Substituted Aryl Imidazole Ligand, Biological Screening and DNA Binding of its Cr(III), Fe(III) and Cu(II) Coordination Compounds as Potential Antibiotic and Anticancer Drugs. *J. Mol. Struct.* **2020**, *1200*, 127034–127045.
10. Jeoung, S.; Kim, S.; Kim, M.; Moon, H. R. Pore Engineering of Metal-Organic Frameworks with Coordinating Functionalities. *Coord. Chem. Rev.* **2020**, *420*, 213377-213392.
11. Aakeroy, C. B.; Champness, N. R.; Janiak, C. Recent Advances in Crystal Engineering. *CrystEngComm* **2010**, *12*, 22–43.
12. Schiebi, J.; Schulmeister, J.; Doppiu, A.; Worner, E.; Rudolph, M.; Karch, R.; Hashmi, A. S. K. An Industrial Perspective on Counter Anions in Gold Catalysis: On Alternative Counter Anions. *Adv. Synth. Catal.* **2018**, *360*, 3949–3954.
13. Khavasi, H. R.; Sadegh, B. M. M. Temperature-Dependent Supramolecular Motif in Coordination Compounds. *Inorg. Chem.* **2010**, *49*, 5356–5358.
14. Bi, W. Y.; Lv, X. Q.; Chai, W. L.; Jin, W. J.; Song, J. R.; Wong, W. K. Synthesis, Structure and Near-Infrared (NIR) Luminescence of Three Solvent-Induced Pseudo-Polymorphic Complexes from a Bimetallic Zn–Nd Schiff-Base Molecular Unit. *Inorg. Chem. Commun.* **2008**, *11*, 1316–1319.
15. Bhattacharyya, M. K.; Saha, U.; Dutta, D.; Das, A.; Verma, A. K.; Frontera, A. Solvent-Driven Structural Topology Involving Energetically Significant Intra- and Intermolecular Chelate Ring Contacts and Anticancer Activities of Cu(II) Phenanthroline Complexes Involving Benzoates: Experimental and Theoretical Studies. *RSC Adv.* **2019**, *9*, 16339–16356.
16. Desiraju, G. R. Chemistry Beyond the Molecule. *Nature* **2001**, *412*, 397–400.

 doi:10.20944/preprints202404.1039.v1

17. Crabtree, R. H. Hypervalency, Secondary Bonding and HB: Siblings Under the Skin. *Chem. Soc. Rev.* **2017**, *46*, 1720–1729.
18. Rather, I. A.; Wagay, S. A.; Ali, R. Emergence of Anion-π Interactions: The Land of Opportunity in Supramolecular Chemistry and Beyond. *Coord. Chem. Rev.* **2020**, *415*, 213327–213386.
19. Bauzá, A.; Frontera, A. σ/π-Hole Noble Gas Bonding Interactions: Insights from Theory and Experiment. *Coord. Chem. Rev.* **2020**, *404*, 213112–213222.
20. Pramanik, S.; Pathak, S.; Frontera, A.; Mukhopadhyay, S. Exploration of Supramolecular and Theoretical Aspects of Two New Cu(II) Complexes: On the Importance of Lone Pair π(Chelate Ring) and π···π(Chelate Ring) Interactions. *J. Mol. Struct.* **2022**, *1265*, 133358–133369.
21. Speetzen, E. D.; Nwachukwu, C. I.; Bowling, N. P.; Bosch, E. Complementary, Cooperative Ditopic Halogen Bonding and Electron Donor-Acceptor π-π Complexation in the Formation of Co-Crystals. *Molecules* **2022**, *27*, 1527-1541.
22. Bhattacharyya, M. K.; Saha, U.; Dutta, D.; Frontera, A.; Verma, A. K.; Sharma, P.; Das, A. Unconventional DNA-Relevant π-Stacked Hydrogen Bonded Arrays Involving Supramolecular Guest Benzoate Dimers and Cooperative Anion–π/π–π/π–Anion Contacts in Coordination Compounds of Co(II) and Zn(II) Phenanthroline: Experimental and Theoretical Studies. *New J. Chem.* **2020**, *44*, 4504–4518.
23. Shmelev, M. A.; Gogoleva, N. V.; Makarov, D. A.; Kiskin, M. A.; Yakushev, I. A.; Dolgushin, F. M.; Aleksandrov, G. G.; Varaksina, E. A.; Taidakov, I. V.; Aleksandrov, E. V.; Sidorov, A. A.; Eremenko, I. L. Synthesis of Coordination Polymers from the Heterometallic Carboxylate Complexes with Chelating N-Donor Ligands. *Russ. J. Coord. Chem.* **2020**, *46*, 1–14.
24. Zhou, Y.; Xu, Y.; Xue, Z.; Shi, J.; Su, Y.; Sun, M.; Wang, S.; Wang, L.; Wang, Q.; Wei, Y. Syntheses, Crystal Structures and Properties of Four Metal Coordination Complexes Constructed from Aromatic Carboxylate and Benzimidazole-Based Ligands. *Transit. Met. Chem.* **2020**, *45*, 353–362.
25. Danilescu, O.; Bulhac, I.; Shova, S.; Novitchi, G.; Bourosh, P. Coordination Compounds of Copper(II) with Schiff Bases Based on Aromatic Carbonyl Compounds and Hydrazides of Carboxylic Acids: Synthesis, Structures, and Properties. *Russ. J. Coord. Chem.* **2020**, *46*, 838–849.
26. Gu, J.; Wan, S.; Kirillova, M. V.; Kirillov, A. M. H-Bonded and Metal(II)-Organic Architectures Assembled from an Unexplored Aromatic Tricarboxylic Acid: Structural Variety and Functional Properties. *Dalton Trans.* **2020**, *49*, 7197–7209.
27. Deegan, C.; McCann, M.; Devereux, M.; Coyle, B.; Egan, D. A. In Vitro Cancer Chemotherapeutic Activity of 1,10-Phenanthroline (phen), $[Ag_2(phen)_3(mal)]\cdot 2H_2O$, $[Cu(phen)_2(mal)]\cdot 2H_2O$ and $[Mn(phen)_2(mal)]\cdot 2H_2O$ ($malH_2$ = Malonic Acid) Using Human Cancer Cells. *Cancer Lett.* **2007**, *247*, 224–233.
28. Prugovečki, B.; Vušak, D.; Ležaić, K.; Jurković, M. Ternary Coordination Compounds of Copper with Amino Acids and 1,10-Phenanthroline–Structural Insight and Biological Activity. *Acta Cryst.* **2021**, *A77*, 975–983.
29. Vušak, D.; Ležaić, K.; Jurec, J.; Žilić, D.; Prugovečki, B. Solvent Effects on the Crystallization and Structure of Ternary Copper(II) Coordination Compounds with L-Threonine and 1,10-Phenanthroline. *Heliyon* **2022**, *8*, 09556-09570.
30. Avdeeva, V. V.; Malinina, E. A.; Zhizhin, K. Y.; Kuznetsov, N. T. Structural Diversity of Cationic Copper(II) Complexes with Neutral Nitrogen-Containing Organic Ligands in Compounds with Boron Cluster Anions and Their Derivatives. *Russ. J. Inorg. Chem.* **2020**, *65*, 514–534.
31. Accorsi, G.; Listorti, A.; Yoosaf, K.; Armaroli, N. 1,10-Phenanthrolines: Versatile Building Blocks for Luminescent Molecules, Materials and Metal Complexes. *Chem. Soc. Rev.* **2009**, *38*, 1690–1700.

32. Teixeira, F. J.; Flores, L. S.; Valverde, T.; Escobar, L. B. L.; Reis, M. S.; Corrêa, C. C. Synthesis and Magnetic Properties of Two Cobalt-Coordination Polymers Containing 1,10-Phenanthroline and Alkyl Dicarboxylates Ligands. *J. Mol. Struct.* **2022**, *1261*, 132820-132835.
33. Romo, A. I. B.; Reis, M. P.; Nascimento, O. R.; Bernhardt, P. V.; Rodríguez-López, J.; Diógenes, I. C. N. Interplay of Electronic and Geometric Structure on Cu Phenanthroline, Bipyridine and Derivative Complexes, Synthesis, Characterization, and Reactivity Towards Oxygen. *Coord. Chem. Rev.* **2023**, *477*, 214943-214960.
34. Bencini, A.; Lippolis, V. 1,10-Phenanthroline: A Versatile Building Block for the Construction of Ligands for Various Purposes. *Coord. Chem. Rev.* **2010**, *254*, 2096–2180.
35. Khan, E. Pyridine Derivatives as Biologically Active Precursors; Organics and Selected Coordination Complexes. *ChemistrySelect* **2021**, *6*, 3041–3064.
36. Raj, D.; Padhi, S. K. The Sporadic μ-Pyridine Bridge in Transition Metal Complexes: A Real Bond or an Interaction? *Coord. Chem. Rev*. **2022**, *450*, 214238–214245.
37. Rao, R. N.; Chanda, K. 2-Aminopyridine–An Unsung Hero in Drug Discovery. *Chem. Commun.* **2022**, *58*, 343–382.
38. Camidge, D. R.; Bang, Y. J.; Kwak, E. L.; Iafrate, A. J.; Varella-Garcia, M.; Fox, S. B.; Riely, G. J.; Solomon, B.; Ou, S. H. I.; Kim, D. W.; Salgia, R. Activity and Safety of Crizotinib in Patients with ALK-Positive Non-Small-Cell Lung Cancer: Updated Results from a Phase 1 Study. *Lancet Oncol.* **2012**, *13*, 1011–1019.
39. Marszaukowski, F.; Guimarães, I. D. L.; da Silva, J. P.; da Silveira Lacerda, L. H.; de Lazaro, S. R.; de Araujo, M. P.; Castellen, P.; Tominaga, T. T.; Boeré, R. T.; Wohnrath, K. Ruthenium (II)-Arene Complexes with Monodentate Aminopyridine Ligands: Insights into Redox Stability and Electronic Structures and Biological Activity. *J. Organomet. Chem.* **2019**, *881*, 66–78.
40. Fisher, M. H.; Lusi, A. Imidazo [1, 2-a] Pyridine Anthelmintic and Antifungal Agents. *J. Med. Chem.* **1972**, *15*, 982–985.
41. Rival, Y.; Grassy, G.; Taudou, A.; Ecalle, R. Antifungal Activity in Vitro of Some Imidazo [1, 2-a] Pyrimidine Derivatives. *Eur. J. Med. Chem.* **1991**, *26*, 13–18.
42. Gudmundsson, K. S.; Johns, B. A. Synthesis of Novel Imidazo [1, 2-a] Pyridines with Potent Activity against Herpesviruses. *Org. Lett.* **2003**, *5*, 1369–1372.
43. Gudmundsson, K. S.; Williams, J. D.; Drach, J. C.; Townsend, L. B. Synthesis and Antiviral Activity of Novel Erythrofuranosyl Imidazo [1, 2-a] Pyridine C-Nucleosides Constructed via Palladium Coupling of Iodoimidazo [1, 2-a] Pyridines and Dihydrofuran. *J. Med. Chem.* **2003**, *46*, 1449–1455.
44. Ismail, M. A.; Brun, R.; Wenzler, T.; Tanious, F. A.; Wilson, W. D.; Boykin, D. W. Novel Dicationic Imidazo [1, 2-a] Pyridines and 5, 6, 7, 8-Tetrahydro-imidazo [1, 2-a] Pyridines as Antiprotozoal Agents. *J. Med. Chem.* **2004**, *47*, 3658–3664.
45. Kaminski, J. J.; Perkins, D. G.; Frantz, J. D.; Solomon, D. M.; Elliott, A. J.; Chiu, P. J. S.; Long, J. F. Antiulcer Agents. 3. Structure-Activity-Toxicity Relationships of Substituted Imidazo [1, 2-a] Pyridines and a Related Imidazo [1, 2-a] Pyrazine. *J. Med. Chem.* **1987**, *30*, 2047–2051.
46. Phukan, N.; Baruah, J. B. Hydrolysis of 4-(4-Oxopentan-2-ylideneamino) Benzoic Acid and In-Situ Formation of Nickel (II), Zinc (II) and Cadmium (II) Complexes of 4-Aminobenzoic Acid. *Inorg. Chim. Acta* **2013**, *396*, 430–435.
47. Dutta, D.; Islam, S. M. N.; Saha, U.; Chetry, S.; Guha, A. K.; Bhattacharyya, M. K. Structural Topology of Weak Non-Covalent Interactions in a Layered Supramolecular Coordination Solid of Zinc Involving 3-Aminopyridine and Benzoate: Experimental and Theoretical Studies. *J. Chem. Crystallogr.* **2018**, *48*, 156–163.

 doi:10.20944/preprints202404.1039.v1

48. Zhang, F.; Lin, Q.-Y.; Zheng, X.-L.; Zhang, L.-L.; Yang, Q.; Gu, J.-W. Crystal Structures, Interactions with Biomacromolecules and Anticancer Activities of Mn(II), Ni(II), Cu(II) Complexes of Demethylcantharate and 2-Aminopyridine. *J. Fluoresc.* **2012**, *22*, 1395–1406.
49. Aitipamula, S.; Nangia, A. Guest-Induced Supramolecular Isomerism in Inclusion Complexes of T-Shaped Host 4,4-Bis(40-Hydroxyphenyl)cyclohexanone. *Chem. Eur. J.* **2005**, *11*, 6727–6742.
50. Liu, K.; Kang, Y.; Wang, Z.; Zhang, X. 25th Anniversary Article: Reversible and Adaptive Functional Supramolecular Materials: "Noncovalent Interaction" Matters. *Advanced Materials* **2013**, *25*, 5530–5548.
51. Morimoto, M.; Bierschenk, S.M.; Xia, K.T.; Bergman, R.G.; Raymond, K.N.; Toste, F.D. Advances in Supramolecular Host-Mediated Reactivity. *Nat Catal* **2020**, *3*, 969–984.
52. Rizzuto, F.J.; von Krbek, L.K.S.; Nitschke, J.R. Strategies for Binding Multiple Guests in Metal–Organic Cages. *Nat Rev Chem* **2019**, *3*, 204–222.
53. Yi, J.W.; Barry, N.P.E.; Furrer, M.A.; Zava, O.; Dyson, P.J.; Therrien, B.; Kim, B.H. Delivery of Floxuridine Derivatives to Cancer Cells by Water-Soluble Organometallic Cages. *Bioconjugate Chem.* **2012**, *23*, 461–471.
54. Yang, Y.-W.; Sun, Y.-L.; Song, N. Switchable Host–Guest Systems on Surfaces. *Acc. Chem. Res.* **2014**, *47*, 1950–1960.
55. Jiang, X.; Yu, H.; Shi, J.; Bai, Q.; Xu, Y.; Zhang, Z.; Hao, X.-Q.; Li, B.; Wang, P.; Wu, L.; et al. From Mechanically Interlocked Structures to Host–Guest Chemistry Based on Twisted Dimeric Architectures by Adjusting Space Constraints. *CCS Chemistry* **2021**, *4*, 2127–2139.
56. Sarma, R.; Karmakar, A.; Baruah, J. B. Synthesis and Characterization of Pyridine N-Oxide Complexes of Manganese, Copper and Zinc. *Inorg. Chim. Acta* **2008**, *361*, 2081–2086.
57. Singh, N. K.; Singh, S. B. Complexes of 1-Isonicotinoyl-4-Benzoyl-3-Thiosemicarbazide with Manganese(II), Iron(III), Chromium(III), Cobalt(II), Nickel(II), Copper(II) and Zinc(II). *Transit. Met. Chem.* **2001**, *26*, 487–495.
58. Etaiw, S. E. H.; El-Bendary, M. M.; Abdelazim, H. Synthesis, Characterization, and Biological Activity of Cd(II) and Mn(II) Coordination Polymers Based on Pyridine-2,6-Dicarboxylic Acid. *Russ. J. Coord. Chem.* **2017**, *43*, 320–330.
59. Wang, C.; Zhang, Y.; Zhang, T. X.; Wang, P.; Gao, S. Four Coordination Compounds Constructed from 1,10-Phenanthroline and Semi-Flexible and Flexible Carboxylic Acids: Hydrothermal Synthesis, Optical Properties and Photocatalytic Performance. *Polyhedron* **2015**, *90*, 58–68.
60. Janiak, C. A Critical Account on π-π Stacking in Metal Complexes with Aromatic Nitrogen-Containing Ligands. *Dalton Trans.* **2000**, *21* 3885–3895.
61. Etter, M. C. Patterns in Hydrogen Bonding: Functionality and Graph Set Analysis in Crystals. *Acc. Chem. Res.* **1990**, *23*, 120–126.
62. Li, S.-L.; Wu, J.-Y.; Tian, Y.-P.; Fun, H.-K.; Chantrapromma, S. Bis(Thio-semicarbazide)Zinc(II) Bis-(Maleate) Dihydrate. *Acta Cryst E* **2005**, *61*, 2701–2703.
63. Wang, Y.; Lin, X. M.; Bai, F. Y.; Sun, L. X. Novel Vanadium Complexes with Rigid Carboxylate Ligands: Synthesis, Structure and Catalytic Bromine Dynamics of Phenol Red. *J. Mol. Struct.* **2017**, *1149*, 379–386.
64. Sharma, R. P.; Saini, A.; Kumar, J.; Kumar, S.; Venugopalan, P.; Ferretti, V. Coordination Complexes of Copper(II) with Herbicide Trichlorophenoxyacetate: Syntheses, Characterization, Single Crystal X-ray Structure and Packing Analyses of Monomeric [Cu(γ-pic)$_3$(2,4,5-Trichlorophenoxyacetate)]·H_2O, [Trans-Cu(en)$_2$(2,4,5-Trichlorophenoxyacetate)$_2$].2H_2O and dimeric [Cu_2(H_2tea)$_2$(2,4,5-Trichlorophenoxyacetate)$_2$]·2(H_2O). *Inorg. Chim. Acta* **2017**, *457*, 59–68.

 doi:10.20944/preprints202404.1039.v1

65. Diab, M. A.; Mohamed, G. G.; Mahmoud, W. H.; El-Sonbati, A. Z.; Morgan, S. M.; Abbas, S. Y. Metal- and Covalent Organic Frameworks as Catalyst for Organic Transformation: Comparative Overview and Future Perspectives. *Appl. Organomet. Chem.* **2019**, *33*, 4945-4962.
66. Nakamoto, K. *Infrared and Raman Spectra of Inorganic and Coordination Compounds*, 5th ed.; John Wiley & Sons: New York, 1997.
67. Tao, J.; Tong, M. L.; Chen, X. M. Hydrothermal Synthesis and Crystal Structures of Three-Dimensional Co-ordination Frameworks Constructed with Mixed Terephthalate (tp) and 4, 4′-Bipyridine (4, 4′-Bipy) Ligands: [M(tp)(4, 4′-Bipy)] (M = Co II, Cd II or Zn II). *J. Chem. Soc., Dalton Trans.* **2000**, *20*, 3669–3674.
68. Titi, A.; Shiga, T.; Oshio, H.; Touzani, R.; Hammouti, B.; Mouslim, M.; Warad, I. Synthesis of Novel Cl2Co4L6 Cluster Using 1-Hydroxymethyl-3, 5-Dimethylpyrazole (LH) Ligand: Crystal Structure, Spectral, Thermal, Hirschfeld Surface Analysis and Catalytic Oxidation Evaluation. *J. Mol. Struct.* **2020**, *1199*, 126995-127010.
69. Bhattacharyya, M. K.; Dutta, D.; Nashre-ul-Islam, S. M.; Frontera, A.; Sharma, P.; Verma, A. K.; Das, A. Energetically Significant Antiparallel π-Stacking Contacts in Co(II), Ni(II), and Cu(II) Coordination Compounds of Pyridine-2,6-dicarboxylates: Antiproliferative Evaluation and Theoretical Studies. *Inorg. Chim. Acta* **2020**, *501*, 119233-119240.
70. Sarma, P.; Gomila, R. M.; Frontera, A.; Barcelo-Oliver, M.; Verma, A. K.; Saikia, S.; Bhattacharyya, M. K. Terephthalato and Succinato Bridged Mn(II) and Zn(II) Coordination Polymers Involving Structure-Guiding H-Bonded Tetrameric Assemblies: Antiproliferative Evaluation and Theoretical Studies. *Polyhedron* **2022**, *224*, 115982-115995.
71. Akyüz, S. The FT-IR Spectra of Transition Metal 3-Aminopyridine Tetracyanonickelate Complexes. *J. Mol. Struct.* **1998**, *449*, 23–27.
72. Shirvan, S. A.; Khazali, F.; Dezfuli, S. H.; Borsalani, A. Distorted Square-Based Pyramidal and Trigonal Bipyramidal Geometries in a Mercury(II) Coordination Compound Containing 2-(Aminomethyl) Pyridine Ligand. *Mol. Cryst. Liq. Cryst.* **2017**, *656*, 105–112.
73. Chan, S.; Wong, W. T. Ruthenium 1992. *Coord. Chem. Rev.* **1995**, *138*, 219–296.
74. Prashanthi, Y.; Kiranmai, K.; Subhashini, N. J. P. Synthesis, Potentiometric and Antimicrobial Studies on Metal Complexes of Isoxazole Schiff Bases. *Spectrochim. Acta Part A* **2008**, *70*, 30–35.
75. Batool, S.S.; Ahmad, S.; Khan, I.U.; Ejaz; Harrison, W.T.A. Structural Characterization of a New Copper(II) Complex of 1,10-Phenanthroline and Benzoate [Cu(Phen)($C_6H_5CO_2^-$)$_2$]. *J Struct Chem* **2015**, *56*, 387–391.
76. Nashre-ul-Islam, S. M.; Dutta, D.; Guha, A. K.; Bhattacharyya, M. K. An Unusual Werner Type Clathrate of Mn(II) Benzoate Involving Energetically Significant Weak CH···C Contacts: A Combined Experimental and Theoretical Study. *J. Mol. Struct.* **2019**, *1175*, 130–138.
77. de Araújo, E. L.; Barbosa, H. F. G.; Dockal, E. R.; Cavalheiro, É. T. G. Synthesis, Characterization and Biological Activity of Cu(II), Ni(II), and Zn(II) Complexes of Biopolymeric Schiff Bases of Salicylaldehydes and Chitosan. *Int. J. Biol. Macromol.* **2017**, *95*, 168–176.
78. Aligo, J. A.; Smith, L.; Eglin, J. L.; Pence, L. E. Solution and Solid-State Variation of Cupric Phenanthroline Complexes. *Inorg. Chem.* **2005**, *44*, 4001–4007.
79. Ekennia, A. C.; Onwudiwe, D. C.; Osowole, A. A.; Olasunkanmi, L. O.; Ebenso, E. E. Synthesis, Biological, and Quantum Chemical Studies of Zn(II) and Ni(II) Mixed-Ligand Complexes Derived from N,N-Disubstituted Dithiocarbamate and Benzoic Acid. *J. Chem.* **2016** *2016* 5129010-5129025.

 doi:10.20944/preprints202404.1039.v1

80. Kalarani, R.; Sankarganesh, M.; Kumar, G. V.; Kalanithi, M. Synthesis, Spectral, DFT Calculation, Sensor, Antimicrobial and DNA Binding Studies of Co(II), Cu(II), and Zn(II) Metal Complexes with 2-Amino Benzimidazole Schiff Base. *J. Mol. Struct.* **2020**, *1206*, 127725-127740.
81. Ghosh, M.; Majee, A.; Nethaji, M.; Chattopadhyay, T. Syntheses and Characterization of trans-[$NiL_2(NCS)_2$][L = 2-(Aminomethyl) Pyridine], trans-[$NiL_2'(NSC)_2$][L′ = 2-(2-Aminoethyl) Pyridine] and trans-[$NiL_2''(NSC)_2$][L″ = 2-(2-Methylaminoethyl) Pyridine] Complexes: X-ray Single Crystal Structure of trans-[$NiL_2'(NSC)_2$][L′ = 2-(2-Aminoethyl) Pyridine]. *Inorg. Chim. Acta* **2009**, *362*, 2052–2055.
82. Yenikaya, C.; Poyraz, M.; Sarı, M.; Demirci, F.; İlkimen, H.; Büyükgüngör, O. Synthesis, Characterization and Biological Evaluation of a Novel Cu(II) Complex with the Mixed Ligands 2,6-Pyridinedicarboxylic Acid and 2-Aminopyridine. *Polyhedron* **2009**, *28*, 3526–3532.
83. Sizova, O. V.; Ershov, A. Y.; Ivanova, N. V.; Shashko, A. D.; Kuteikina-Teplyakova, A. V. Ru(II) Chloro-bis(bipyridyl) Complexes with Substituted Pyridine Ligands: Interpretation of Their Electronic Absorption Spectra. *Russ. J. Coord. Chem.* **2003**, *29*, 494–500.
84. de Mesquita, M. E.; Junior, S. A.; Oliveira, F. C.; Freire, R. O.; Júnior, N. B. C.; De Sá, G. F. Synthesis, Spectroscopic Studies and Structure Prediction of the New $Tb(3\text{-}NH_2PIC)_3{\cdot}3H_2O$ Complex. *Inorg. Chem. Commun.* **2002**, *5*, 292–295.
85. Batool, S.S.; Harrison, W.T.A.; Syed, Q.; Haider, M.S. Syntheses and Crystal Structures of Mixed-Ligand Copper(II)–Imidazole–Carboxylate Complexes. *Journal of Coordination Chemistry* **2018**, *71*, 1380–1391.
86. Nath, H.; Sharma, P.; Frontera, A.; Barcelo-Oliver, M.; Verma, A.K.; Das, J.; Bhattacharyya, M.K. Phenanthroline-Based Ni(II) Coordination Compounds Involving Unconventional Discrete Fumarate-Water-Nitrate Clusters and Energetically Significant Cooperative Ternary π-Stacked Assemblies: Antiproliferative Evaluation and Theoretical Studies. *Journal of Molecular Structure* **2022**, *1248*, 131424-131440.
87. Yang, Q.; Chen, S.; Gao, S. Two Mn(II) Chloride Complexes Containing Guest Molecules. *J Therm Anal Calorim* **2007**, *89*, 567–571.
88. Al-Fakeh, M.S.; Allazzam, G.A.; Yarkandi, N.H. Ni(II), Cu(II), Mn(II), and Fe(II) Metal Complexes Containing 1,3-Bis(Diphenylphosphino)Propane and Pyridine Derivative: Synthesis, Characterization, and Antimicrobial Activity. *International Journal of Biomaterials* **2021**, *2021*, 4981367-4981381.
89. Porterfield, J.P.; Bross, D.H.; Ruscic, B.; Thorpe, J.H.; Nguyen, T.L.; Baraban, J.H.; Stanton, J.F.; Daily, J.W.; Ellison, G.B. Thermal Decomposition of Potential Ester Biofuels. Part I: Methyl Acetate and Methyl Butanoate. *J. Phys. Chem. A* **2017**, *121*, 4658–4677.
90. SADABS, V2.05 and Bruker AXS, Madison, USA, 1999.
91. Sheldrick, G.M. Crystal Structure Refinement with SHELXL. *Acta Crystallogr., Sect. A: Found. Crystallogr.* **2008**, *64*, 112–117.
92. Farrugia, L.J. WinGX and ORTEP for Windows: An Update. *J. Appl. Cryst.* **2012**, *45*, 849–854.
93. Brandenburg, K. Diamond 3.1f. Crystal Impact GbR: Bonn, Germany, 2008.
94. Ahlrichs, R.; Bär, M.; Häser, M.; Horn, H.; Kölmel, C. Electronic Structure Calculations on Workstation Computers: The Program System TURBOMOLE. *Chem. Phys. Lett.* **1989**, *162*, 165–169.
95. A. D. Becke, Phys. Rev. A, **1988**, *38*, 3098-100.
96. E. Caldeweyher, J.-M. Mewes, S. Ehlert, S. Grimme, Phys. Chem. Chem. Phys., **2020**, *22*, 8499-8512.
97. F. Weigend, Phys. Chem. Chem. Phys. **2006**, *8*, 1057–1065.
98. R. F. W. Bader, Chem. Rev. **1991**, *91*, 893–928.

 doi:10.20944/preprints202404.1039.v1

99. E. R. Johnson, S. Keinan, P. Mori-Sánchez, J. Contreras-García, A. J. Cohen, W. Yang, J. Am. Chem. Soc. **2010**, *132*, 6498-6506

100. T. Lu, F. Chen, J. Comput. Chem. **2012**, *33*, 580–592.

101. J. W. Humphrey, A. Dalke, K. Schulten, J. Mol. Graphics **1996**, *14*, 33–38.